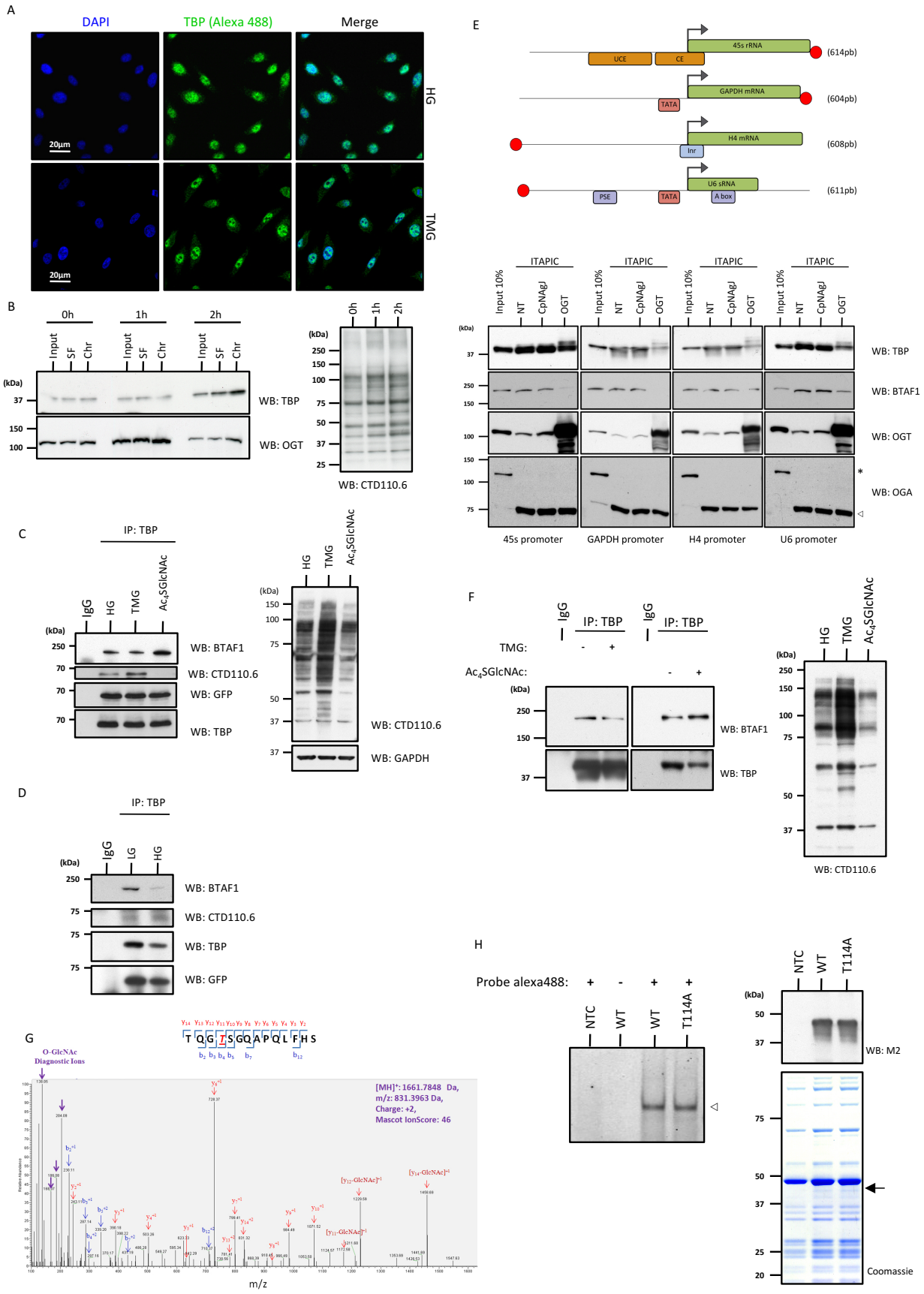
A
DAPI
TBP (Alexa 488)
Merge
HG
TMG
20µm
B
0h
1h
2h
Input
SF
Chr
(kDa)
WB: TBP
WB: OGT
WB: CTD110.6
C
IP: TBP
IgG
HG
TMG
Ac4SGlcNAc
WB: BTAF1
WB: CTD110.6
WB: GFP
WB: TBP
WB: GAPDH
D
IP: TBP
IgG
LG
HG
WB: BTAF1
WB: CTD110.6
WB: TBP
WB: GFP
G
O-GlcNAc
Diagnostic Ions
T Q G T S G Q A P Q L F H S
[MH]+: 1661.7848 Da,
m/z: 831.3963 Da,
Charge: +2,
Mascot IonScore: 46
m/z
E
45s rRNA
(614pb)
UCE
CE
GAPDH mRNA
(604pb)
TATA
H4 mRNA
(608pb)
Inr
U6 sRNA
(611pb)
PSE
TATA
A box
ITAPIC
Input 10%
NT
CpNAgJ
OGT
WB: TBP
WB: BTAF1
WB: OGT
WB: OGA
45s promoter
GAPDH promoter
H4 promoter
U6 promoter
F
IgG
IP: TBP
TMG:
Ac4SGlcNAc:
WB: BTAF1
WB: TBP
HG
TMG
Ac4SGlcNAc
WB: CTD110.6
H
Probe alexa488:
NTC
WT
T114A
WB: M2
Coomassie

Figure S1: related to Figure 1

(A) Effect of TMG treatment on TBP cellular localization in HeLa cells. (B) TMG treatment increased TBP interaction with chromatin. Cells were incubated for the indicated time with TMG. Input, DNA-bound protein fraction (Chr) and soluble protein fraction (SF) were immunoblotted with indicated antibodies (left panel). TMG effect on total protein O-GlcNAcylation was normalized to total cell lysate (right panel). (C) Effect of TMG and Ac_4SGlcNAc on GFP-TBP O-GlcNAcylation and BTAF1 interaction (left panel). Effect of each inhibitors on global O-GlcNAcylation by Western blot (right panel). (D) O-GlcNAcylation of GFP-TBP and its ability to interact with BTAF1 under different glucose conditions. (E) *In vitro* immobilized template analysis of PIC assembly (ITAPIC). Schematic representation of the organization of the selected promoters with the position of the biotin (red bullet) used for *in vitro* PIC assembly (upper panel). Immunoblots of TBP, BTAF1, OGT and OGA enrichment in ITAPIC on the indicated promoter (lower panel). * and ◁ point expected molecular weight corresponding to OGA full length and a shorter OGA isoform respectively. (F) TMG or Ac_4SGlcNAc treatment of HeLa cells decreased or increased co-precipitation of BTAF1 with TBP, respectively. BTAF1 was co-immunoprecipitated with TBP (left panel). Effect of TMG and Ac_4SGlcNAc on protein O-GlcNAcylation (right panel). (G) CID/HCD spectrum of a peptide covering the T114-O-GlcNAc. (H) EMSA of TBP wild-type and O-GlcNAc T114A mutant (left panel, ◁ indicates TBP:DNA complex). Production by coupled *in vitro* transcription/translation of 3X-FLAG tagged TBP wild-type and its mutant version (right panels). M2 3XFLAG immunoblot and Coomassie staining (Arrow indicates band corresponding to TBP).

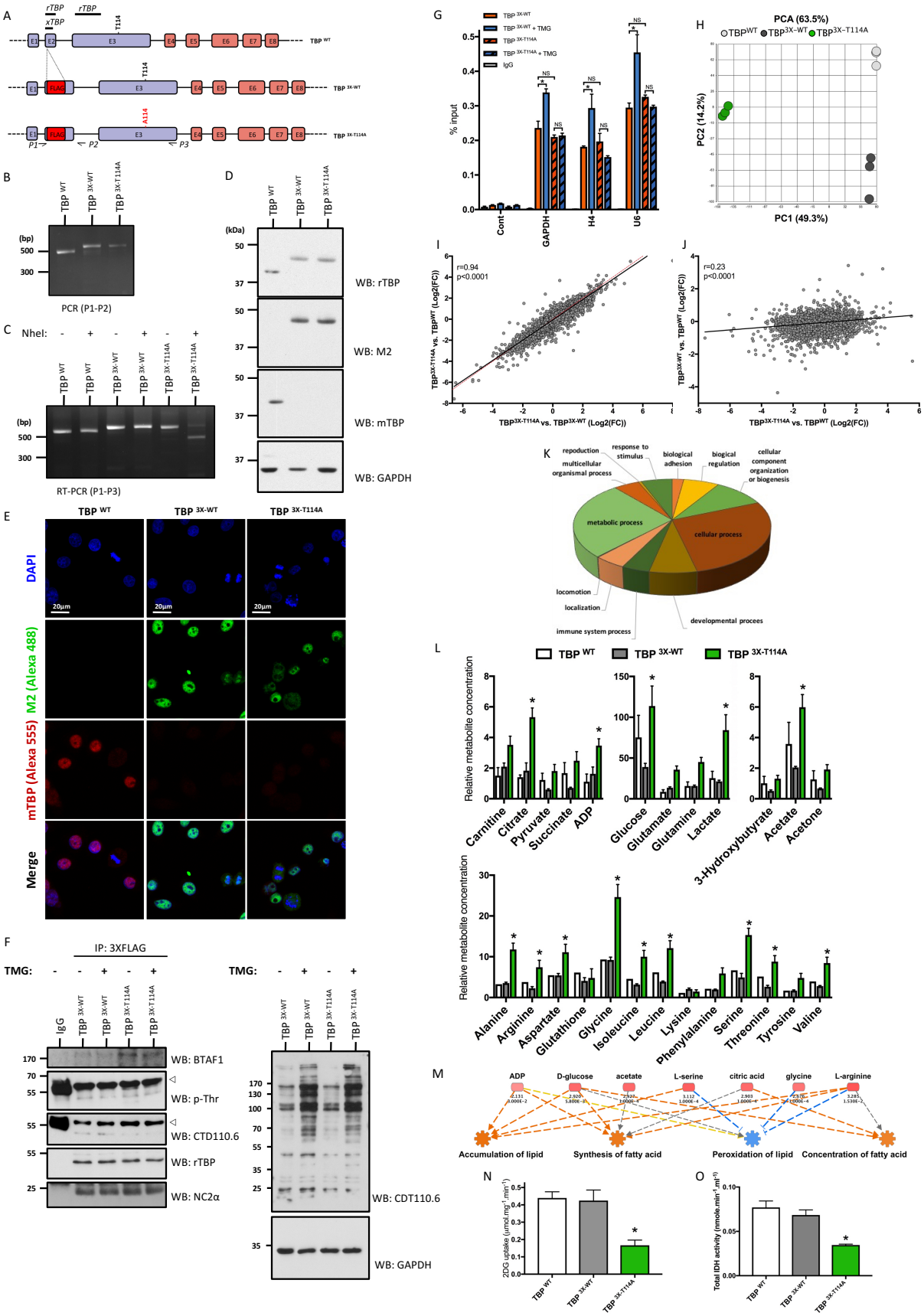
A
rTBP
rTBP
xTBP
T114
A114
E1
E2
E3
E4
E5
E6
E7
E8
FLAG
TBP WT
TBP 3X-WT
TBP 3X-T114A
P1
P2
P3
B
PCR (P1-P2)
(bp)
500
300
C
NheI:
RT-PCR (P1-P3)
D
(kDa)
50
37
WB: rTBP
WB: M2
WB: mTBP
WB: GAPDH
E
DAPI
M2 (Alexa 488)
mTBP (Alexa 555)
Merge
20μm
F
IP: 3XFLAG
TMG:
IgG
WB: BTAF1
WB: p-Thr
WB: CTD110.6
WB: rTBP
WB: NC2α
WB: CDT110.6
WB: GAPDH
G
TBP 3X-WT + TMG
TBP 3X-T114A + TMG
IgG
% input
NS
Cont
GAPDH
H4
U6
H
PCA (63.5%)
PC2 (14.2%)
PC1 (49.3%)
I
r=0.94
p<0.0001
TBP3X-T114A vs. TBPWT (Log2(FC))
TBP3X-T114A vs. TBP3X-WT (Log2(FC))
J
r=0.23
p<0.0001
TBP3X-WT vs. TBPWT (Log2(FC))
TBP3X-T114A vs. TBPWT (Log2(FC))
K
repoduction
multicellular organismal process
response to stimulus
biological adhesion
biogical regulation
cellular component organization or biogenesis
metabolic process
cellular process
locomotion
localization
immune system process
developmental procees
L
Relative metabolite concentration
Carnitine
Citrate
Pyruvate
Succinate
ADP
Glucose
Glutamate
Glutamine
Lactate
3-Hydroxybutyrate
Acetate
Acetone
Alanine
Arginine
Aspartate
Glutathione
Glycine
Isoleucine
Leucine
Lysine
Phenylalanine
Serine
Threonine
Tyrosine
Valine
M
ADP
D-glucose
acetate
L-serine
citric acid
glycine
L-arginine
Accumulation of lipid
Synthesis of fatty acid
Peroxidation of lipid
Concentration of fatty acid
N
2DG uptake (μmol.mg-1.min-1)
O
Total IDH activity (nmole.min-1.ml-1)

Figure S2: Related to Figure 2

(A) Schematic representation of the *TBP* gene edition. First 3X-FLAG tag has been inserted in frame in the exon 2 after the endogenous start codon of TBP in order to disrupt a well characterized anti-TBP antibody to track wild-type TBP and its edited counterpart. Then exon 3 that encodes the area containing the T114 mapped O-GlcNAc site of TBP has been targeted and the codons of the T114 and the T115 were respectively engineered to code for an alanine and for threonine with a silent mutation generating a NheI restriction site for screening purposes. (B) Genomic PCR of the area spanning exon 2 of *TBP*. (C) RT-PCR validation of the insertion of the 3XFLAG tag and the edition of the codons T114 and T115. (D) Expression level of endogenous TBP and its edited versions. Cell lysates were immunoblotted with indicated antibodies. (E) Cellular localization of TBP^{WT}, $TBP^{3X\text{-}WT}$ and $TBP^{3X\text{-}T114A}$. Immunostaining was performed with the indicated antibodies and dyes. (F) O-GlcNAcylation and threonine phosphorylation levels of HeLa CRISPR edited $TBP^{3X\text{-}WT}$ and $TBP^{3X\text{-}T114A}$ and their ability to interact with BTAF1 and NC2α under 25 mM glucose treated or not with TMG (left panels); ◁ indicates IgG. Effect of TMG on global O-GlcNAcylation level (right panel). (G) CRISPR edited $TBP^{3X\text{-}WT}$ and $TBP^{3X\text{-}T114A}$ promoter occupancy on *GAPDH*, *H4* and *U6* promoter treated or not with TMG. Data are mean ± SEM, $n \geq 2$, $^*p < 0.05$, NS: not significant. (H) Principal component analysis of the RNA-Seq data of TBP^{WT}, $TBP^{3X\text{-}WT}$ and $TBP^{3X\text{-}T114A}$ cells (n = 3). (I) Scatterplot comparing Log2(FC) of gene expression profiling of $TBP^{3X\text{-}T114A}$ to both wild-type cells. Solid black line shows linear correlation and red dash line represent perfect correlation. (J) Scatterplot comparing Log2(FC) of gene expression profiling of $TBP^{3X\text{-}T114A}$ and $TBP^{3X\text{-}WT}$ to TBP^{WT} cell line. Solid black line shows linear correlation. (K) GO analysis of differentially express transcripts between $TBP^{3X\text{-}T114A}$ and $TBP^{3X\text{-}WT}$ cells. (L) Metabolomics analysis of the TBP^{WT}, $TBP^{3X\text{-}WT}$ and $TBP^{3X\text{-}T114A}$ cells by ^{1}H-NMR normalized to total protein. Data are mean ± SEM, n = 3, $^*p < 0.05$

compared to both wild-type cells. (M) IPA representation showing the upregulation prediction function pathways of accumulation of lipids, synthesis of fatty acids, concentration of fatty acids, and downregulation of peroxidation of lipids. (N) 2-doxyglucose (2DG) uptake in TBP^{WT}, $TBP^{3X\text{-}WT}$ and $TBP^{3X\text{-}T114A}$ cells. Data are mean ± SEM, n = 4, *p <0.05 compared to both wild-type cells. (O) Total IDH activity in $TBP^{3X\text{-}T114A}$ and $TBP^{3X\text{-}WT}$ to TBP^{WT} cells. Data are mean ± SD, n = 3, *p <0.05 compared to both TBP^{WT} and $TBP^{3X\text{-}WT}$.

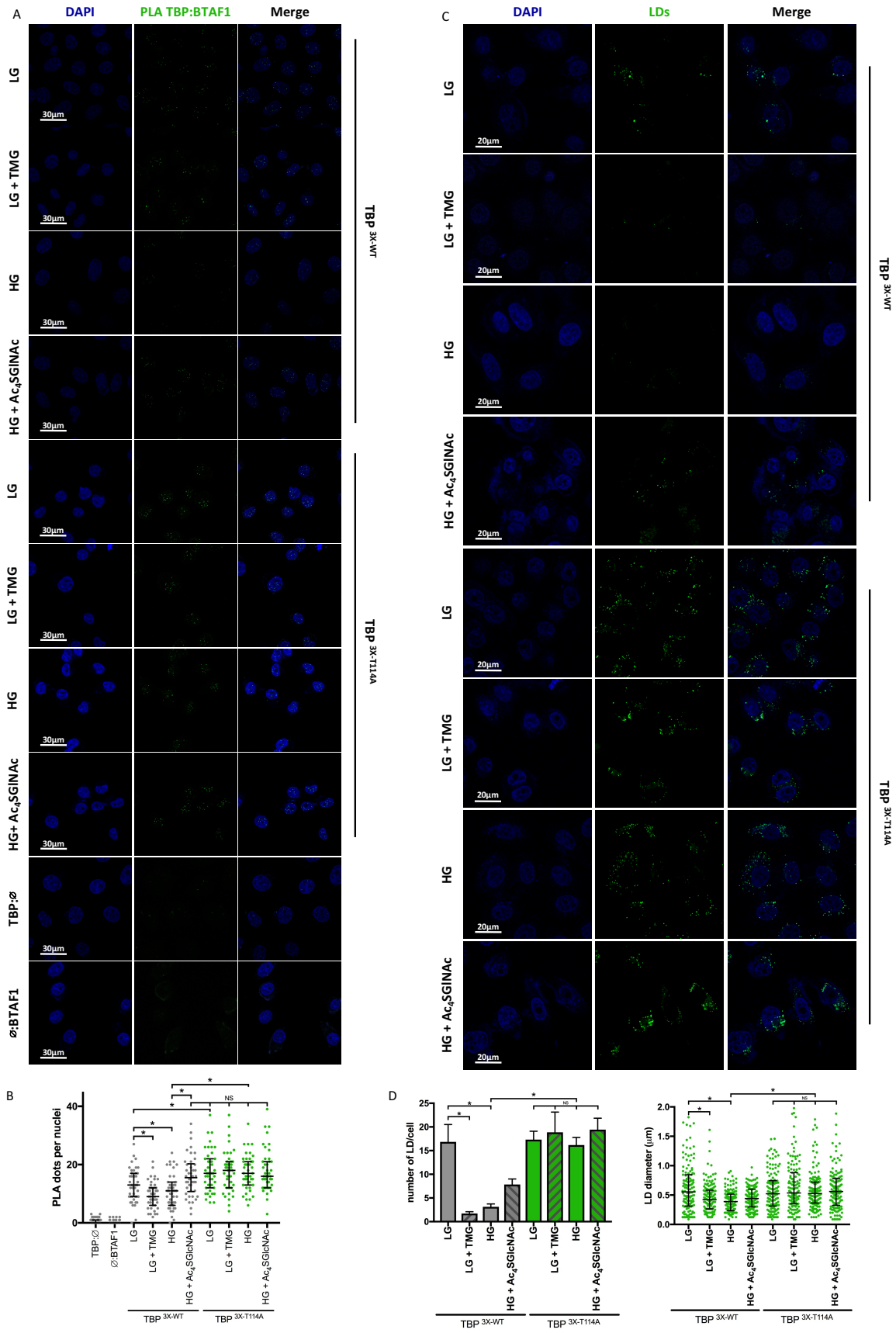
A
DAPI
PLA TBP:BTAF1
Merge
LG
LG + TMG
HG
HG + Ac4SGlNAc
LG
LG + TMG
HG
HG+ Ac4SGlNAc
TBP:∅
∅:BTAF1
30µm
TBP 3X-WT
TBP 3X-T114A
C
DAPI
LDs
Merge
LG
LG + TMG
HG
HG + Ac4SGlNAc
LG
LG + TMG
HG
HG + Ac4SGlNAc
20µm
TBP 3X-WT
TBP 3X-T114A
B
PLA dots per nuclei
TBP:∅
∅:BTAF1
LG
LG + TMG
HG
HG + Ac4SGlNAc
LG
LG + TMG
HG
HG + Ac4SGlNAc
TBP 3X-WT
TBP 3X-T114A
NS
D
number of LD/cell
LD diameter (µm)
LG
LG + TMG
HG
HG + Ac4SGlNAc
LG
LG + TMG
HG
HG + Ac4SGlNAc
TBP 3X-WT
TBP 3X-T114A
NS

Figure S3: Related to Figure 3

(A) *In situ* interaction of TBP:BTAF stained with proximity ligation assay (PLA) in $TBP^{3X\text{-}WT}$ and $TBP^{3X\text{-}T114A}$ cells under 5.5- or 25mM glucose treated or not with TMG or $Ac_4SGlcNAc$. (B) Quantification of PLA signal. Number of PLA dots per nuclei are shown as median with interquartile range (n = 3, total of 43 cells per condition were measured), *p < 0.05, NS: not significant. (C) LDs staining of indicated cells under 5.5- or 25 mM glucose treated or not with TMG or $Ac_4SGlcNAc$. (D) Quantitative analysis of the LD number per cell (left panel) and size (right panel) of Figure S3K. Number of LD per cell are shown as mean ± SEM (n ≥ 3), NS: not significant. LDs size data are median with interquartile range (n ≥ 3, total of 134 LDs were measured per condition), *p < 0.05.

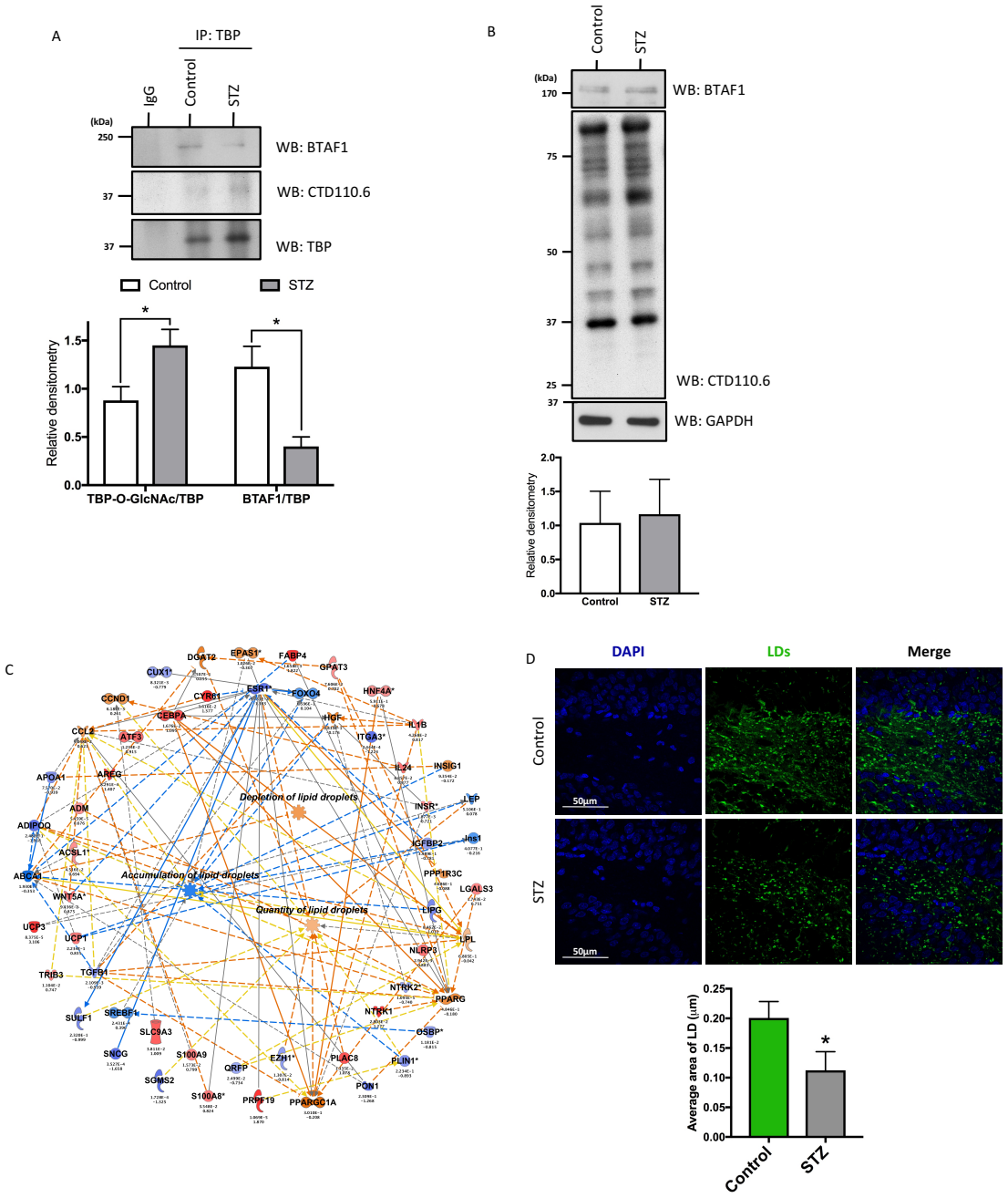

Figure S4: Related to Figure 4

(A) Effect of STZ-induced hyperglycemia on TBP:BTAF1 interaction in rat brain. BTAF1 was co-immunoprecipitated along with TBP by TBP antibody. Samples were immunoblotted with indicated antibodies (top panel). Densitometry analysis of TBP-O-GlcNAc and TBP:BTAF1 interaction in STZ-treated rat brain (bottom panel). Data are mean ± SEM, n = 5 rats per group, *p

< 0.05. (B) Effect of STZ-induced hyperglycemia on global protein O-GlcNAcylation and BTAF1 expression in rat brain (top panel). Relative densitometry analysis of BTAF1 protein level in control and STZ injected rat (Bottom panel). Data are mean ± SEM, n = 3 rats per group. (C) IPA representation showing upregulation prediction function pathways of accumulation, quantity and depletion of LDs. Network built using hippocampal transcriptomic data set of STZ treated rats from GSE34451 (Abdul-Rahman et al., 2012). (D) LDs staining of rat hippocampus treated with STZ or vehicle (top panel). Relative quantification of LDs in rat hippocampus (bottom panel), Data are mean ± SEM, n = 5 rats per group, *p < 0.05.